Ceramics International 49 (2023) 26803–26810

Contents lists available at ScienceDirect

Ceramics International

journal homepage: www.elsevier.com/locate/ceramint

Novel $AMoO_4:Eu^{3+}$ (A = Ca and Ba) optical thermometer: Investigation of effect of local ionic coordination environment on optical performance and temperature measurement sensitivity

Huabo Gao [a], Maxim S. Molokeev [b,c,d], Qi Chen [a], Xin Min [e], Bin Ma [a,*]

[a] School of Mechanical Engineering, Qinghai University, Xining, 810016, China
[b] Laboratory of Crystal Physics, Kirensky Institute of Physics, Federal Research Center KSC SB RAS, Krasnoyarsk, 660036, Russia
[c] Siberian Federal University, Krasnoyarsk, 660041, Russia
[d] Department of Physics, Far Eastern State Transport University, Khabarovsk, 680021, Russia
[e] Beijing Key Laboratory of Materials Utilization of Nonmetallic Minerals and Solid Wastes, National Laboratory of Mineral Materials, School of Materials Science and Technology, China University of Geosciences (Beijing), Beijing, 100083, China

ARTICLE INFO

Handling Editor: Dr P. Vincenzini

Keywords:
Phosphor
Optical thermometer
Coordination environment
Abnormal thermal quenching

ABSTRACT

A range of Eu^{3+}-doped $AMoO_4$ (A = Ca and Ba) phosphors were successfully synthetized, and their crystal structures, optical performance, and temperature measurement sensitivities were investigated in detail. Peak doping concentration of $CaMoO_4:Eu^{3+}$ phosphor was 0.18, while peak doping concentration of $BaMoO_4:Eu^{3+}$ phosphor may be greater than 0.18. Then, temperature-dependent photoluminescence emission spectra of representative $CaMoO_4:0.09Eu^{3+}$ and $BaMoO_4:0.03Eu^{3+}$ phosphors were recorded. $CaMoO_4:0.09Eu^{3+}$ phosphor exhibited abnormal thermal quenching, which was attributed to defects caused by heterovalent substitution of ions and increase in the temperature, and good thermal stability. Finally, the possibility of using both phosphors as optical thermometers was discussed, which exhibited good temperature sensitivity. However, $CaMoO_4:0.09Eu^{3+}$ phosphor exhibited two peak absolute (Sa, 1.28 $\%K^{-1}$ and 1.39 $\%K^{-1}$) and relative sensitivities (Sr, 1.21 $\%K^{-1}$ and 1.20 $\%K^{-1}$). In addition, variation trend of Sr value with temperature was considerably peculiar. Two optimum Sa and Sr values were attributed to abnormal thermal quenching of $CaMoO_4:0.09Eu^{3+}$ phosphor. Peak Sa and Sr values of $BaMoO_4:0.03Eu^{3+}$ phosphor was 12.39 $\%K^{-1}$ and 0.89 $\%K^{-1}$, respectively. In addition, Sa of $AMoO_4:Eu^{3+}$ phosphor was negatively related to Eu^{3+} central asymmetry, while peak Sr value was more inclined to appropriate ionic central asymmetry.

1. Introduction

As an essential thermodynamic parameter, temperature is a key index or parameter in numerous fields, such as scientific research, biomedicine, industrial manufacturing, and daily life. Accurate measurement of temperature is vital for practical applications. However, traditional thermometers based on the contraction principle exhibit disadvantages of a long response time and easy interference by environmental factors, and the corresponding measurement results exhibit a certain dependence on environmental factors. As a result, conventional thermometers do not meet some of the harshest practical requirements. Hence, a novel type of a non-contact thermometer with high detection resolution and accuracy as well as excellent sensitivity is required [1–3].

In this regard, optical thermometers based on the fluorescence intensity ratio (FIR) have attracted considerable research attention recently [4–6]. FIR technology is based on a pair of thermally (or non-thermally) coupled energy levels (TCL or NTCL) of rare-earth (RE) ions. FIR technology based on the latter typically combines the energy-transfer (ET) effect, demonstrating a prominent effect on improvement of the detection sensitivity of optical thermometers [7,8]. Typically, phosphors co-doped with RE ions are designed by the energy transfer between them, and single-doped phosphors are designed by the energy transfer from the host to the doped ions. For example, Du et al. [9] investigated the $Ba_3(VO_4)_2:Sm^{3+}$ optical thermometer with energy transfer ($VO_4^{3-} \rightarrow Sm^{3+}$), exhibiting the maximum absolute sensitivity and relative sensitivity (Sa and Sr) of 3.9 $\%K^{-1}$ and 2.24 $\%K^{-1}$, respectively. Yang et al. [10] designed a $Y_3Ga_5O_{12}:xEu^{3+},yTb^{3+}$ optical thermometer based on energy transfer ($Ga^{3+} \rightarrow Tb^{3+} \rightarrow Eu^{3+}$) and NTCL,

* Corresponding author.
E-mail address: bin.m@qhu.edu.cn (B. Ma).

https://doi.org/10.1016/j.ceramint.2023.05.217
Received 8 February 2023; Received in revised form 16 May 2023; Accepted 23 May 2023
Available online 24 May 2023

with optimal Sa and Sr values of 2.8 $\%K^{-1}$ and 7.03 $\%K^{-1}$, respectively. Khajuria et al. [11] investigated TCL- and NTCL-based $Na_3Y(PO_4)_2$:Yb^{3+},Er^{3+} optical thermometers and reported that Sa (16 $\%K^{-1}$) and Sr (0.8 $\%K^{-1}$) values of the latter were higher and that its performance was better for optical temperature measurement. Compared to the optical thermometer based on TCL FIR technology [12,13], the above novel thermometers undoubtedly exhibit a better detection sensitivity. Although several studies on optical thermometers have been reported, and these optical thermometers have excellent sensitivity, it is still essential to further improve the sensitivity of luminescent thermometers, broaden their types, and investigate latent factors that affect their temperature measurement sensitivities.

An optical thermometer is well known to be based on a phosphor or fluorescent material. Hence, its temperature measurement sensitivity is inevitably affected by photoluminescence properties. As a vital element in the family of RE, europium (Eu) is used as an activator of different hosts and generates red luminescence in the visible region [14,15]. Studies have reported that effects of different coordination environments of Ln^{3+} on its optical performance cannot be ignored [16,17]. For Eu^{3+}, the typical transitions $^5D_0 \rightarrow {}^7F_J$ (J = 1, 2, 3) are extremely sensitive to its coordination environment. Based on the Judd–Ofelt theory, if Eu^{3+} occupies a lattice with high central symmetry, the magnetic dipole transition ($^5D_0 \rightarrow {}^7F_1$) will dominate Eu^{3+} emissions; else, the electric dipole transition ($^5D_0 \rightarrow {}^7F_2$) will dominant. The proportion of ($^5D_0 \rightarrow {}^7F_2$)/($^5D_0 \rightarrow {}^7F_1$) represents the deviation between the actual local coordination environment of Eu^{3+} and absolute central symmetric site [15,18]. Therefore, it is crucial to investigate the effect of ionic local coordination environment differences on the optical performance or the temperature measurement sensitivity of optical thermometers.

Previously, our group has prepared phosphors based on a pair of NTCL and energy transfer ($Mo(W)O_4^{2-} \rightarrow Eu^{3+}$) and systematically investigated the effect of the ionic coordination environment on the temperature measurement sensitivity of phosphors [19]. Considering that the different anionic groups selected for research may exhibit a certain deviation in action, in this study, a range of $AMoO_4:Eu^{3+}$ (A = Ca and Ba) phosphors were prepared using the same anionic group and adjusting the type of cations. In these phosphors, Eu^{3+} occupies the Ca^{2+} or Ba^{2+} sites rather than Mo^{6+} sites. Finally, the optical performance of $AMoO_4:Eu^{3+}$ phosphor and the effects of different ionic coordination environments on the temperature measurement sensitivity were investigated.

2. Experimental

2.1. Sample synthesis

A range of $AMoO_4:Eu^{3+}$ (A = Ca and Ba) phosphors were prepared by the conventional solid-state method using original materials such as Eu_2O_3 (99.99%), MoO_3 (99.5%), $BaCO_3$ (99.0%), and $CaCO_3$ (99.0%). All of these original materials were used directly without further processing. For phosphor preparation, the original materials at an appropriate stoichiometric ratio were weighed, completely mixed, and ground. Next, the samples were pre-calcined at 850 °C for 5 h (low-temperature box furnace) and calcined at 1200 °C for 5 h (high-temperature tube furnace). The product was completely ground to obtain the final sample.

2.2. Characterization and measurements

The phase structures of samples were identified by an X-ray diffraction (D8 Advance diffraction). The morphology and element type of samples were identified by a field-emission scanning electron microscopy (JSM-7900F). The PLE and PL spectra of samples were recorded on a 150-W Xe fluorescence spectrophotometer (F-7100) with a heating controller. The fluorescence decay curves and fluorescence lifetimes of samples were recorded on a Fluoro Cube NL system (HORIBA).

3. Results and discussion

3.1. Structure and morphology analysis

The XRD patterns of the as-obtained $CaMoO_4:Eu^{3+}$ and $BaMoO_4:Eu^{3+}$ samples are demonstrated in Fig. 1(a) and (b), respectively. Apparently, all diffraction peaks are well indexed to their standard patterns (JCPDS No. 85–585 and No. 29–193), without clear impurity diffraction peaks, indicating that all samples exhibit pure phases. Based on the similar ionic radii (when coordination number (CN) = 8, Ca^{2+} = 1.12 Å, Ba^{2+} = 1.42 Å, Eu^{3+} = 1.066 Å) [20–22], Eu^{3+} doping does not cause prominent variation in the crystal structure. XRD Rietveld refinement analysis of pure $CaMoO_4$ was also conducted. The good agreement between original data and the calculated results, as well as small reliability factors, including 10.91 (R_{wp}), 8.39 (R_p), 4.45 (R_B), and 2.22 (χ^2), indicated that $CaMoO_4$ host sample is successfully synthesized (Fig. 1(c)). The calculated lattice parameters are a = b = 5.2263 Å, c = 11.4371 Å, α = β = γ = 90°, V = 312.395 $Å^3$. As shown in Fig. 1(d), the $AMoO_4$ crystal structure exhibits a typical scheelite structure and a uniform space group ($I4_1/a$), comprising a MoO_4 tetrahedron and an AO_8 dodecahedron.

Fig. 2(a) and (f) shows the SEM images of representative $AMoO_4:0.06Eu^{3+}$ phosphor. Clearly, the phosphors are composed of irregular particles. Fig. 2(b-e) and (g-j) show the corresponding elemental mapping images of $AMoO_4:0.06Eu^{3+}$ phosphor. Ca (or Ba), Mo, O, and Eu are uniformly covered on the particle surface. The above results indicated that the target phosphors are synthesized successfully.

3.2. Optical performance analysis

Clearly, at an emission wavelength of 616 nm, $AMoO_4:Eu^{3+}$ phosphors exhibit several characteristic absorption peaks located at ~362, 382, 394, and 416 nm, which are attributed to $^7F_0 \rightarrow {}^5D_4$, $^7F_0 \rightarrow {}^5L_4$, $^7F_0 \rightarrow {}^5L_6$, and $^7F_0 \rightarrow {}^5D_3$ transitions of Eu^{3+}, respectively (Fig. 3) [23,24]. Particularly, for $BaMoO_4:Eu^{3+}$ phosphor, a $^7F_0 \rightarrow {}^5D_2$ transition is observed near 464 nm, while that for the $CaMoO_4:Eu^{3+}$ phosphor is almost invisible. In addition, dominant peaks are observed at different positions, which are located at 394 nm and 464 nm respectively, indicating that the same activator ions under different coordination environments may exhibit different major absorption peaks; that is, the sensitivity to excitation light is not consistent [18]. Notably, a wide absorption band observed at 250–350 nm is attributed to the charge transfer from O^{2-} to Eu^{3+}, and the wide absorption band is also called the charge-transfer state band (CTB) [25,26].

As shown in Fig. 4(a) and (b), under the excitation wavelengths of 309 and 291 nm, the sharp emission peaks centered at ~466, 537, 593, 616, and 656 nm are attributed to $^5D_2 \rightarrow {}^7F_0$, $^5D_1 \rightarrow {}^7F_1$, $^5D_0 \rightarrow {}^7F_1$, $^5D_0 \rightarrow {}^7F_2$, and $^5D_0 \rightarrow {}^7F_3$ transitions, respectively [10,27], which are consistent with the characteristic transitions of Eu^{3+}. In addition, the wide emission bands at 400–575 nm are attributed to the $^3T_{1,\ 2} \rightarrow {}^1A_1$ characteristic transition of MoO_4^{2-} group [28]. In addition, compared with that of the pure $AMoO_4$ host, the emission intensity of the host doped with Eu^{3+} decreases, confirming the energy transfer of $MoO_4^{2-} \rightarrow Eu^{3+}$. Notably, for $BaMoO_4$ host, the PL spectrum shows the characteristic emission of Eu^{3+}, which may be attributed to the fact that a small amount of Eu^{3+} volatilized into the pure host sample when the BaMoO4:Eu^{3+} phosphor samples were synthesized in the same batch. The International Commission on illumination (CIE) chromatic coordinates of all synthesized phosphors are shown in Fig. 4(c) and (d), exhibiting pink- and purple-light emissions, respectively.

For $CaMoO_4:Eu^{3+}$ phosphor, at a Eu^{3+} content of 0.18, the PL emission intensity peaks and then decrease with increasing doping content (Fig. 5(a)). This result may be attributed to concentration quenching (CQ) at 0.18 [29–31], that is, the peak activator doping

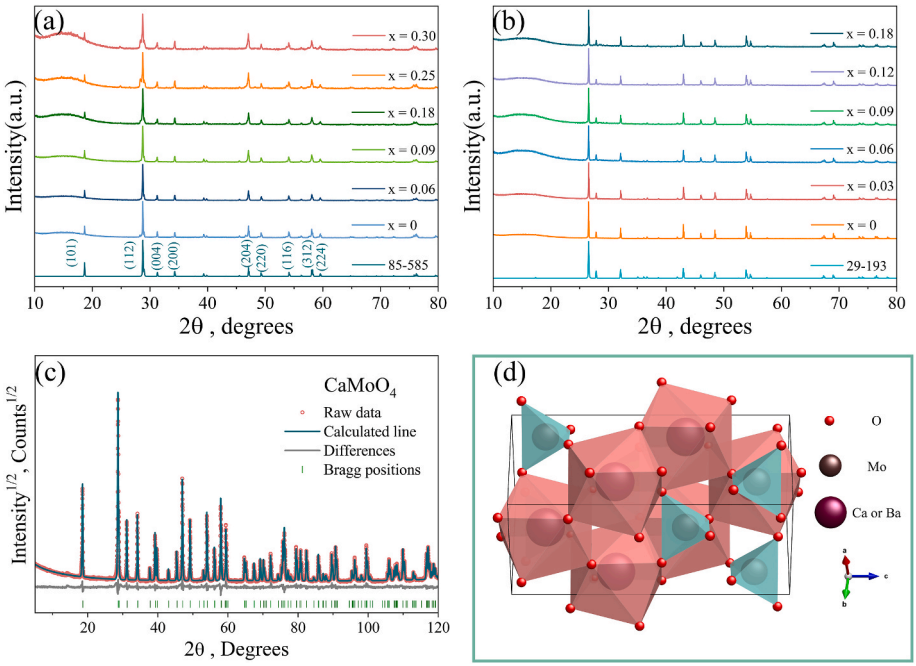

Fig. 1. XRD patterns of (a) $CaMoO_4$:xEu^{3+} and (b) $BaMoO_4$:xEu^{3+} phosphors. (c) Rietveld refinement results of a pure $CaMoO_4$ sample. (d) Crystal structure of $AMoO_4$ host.

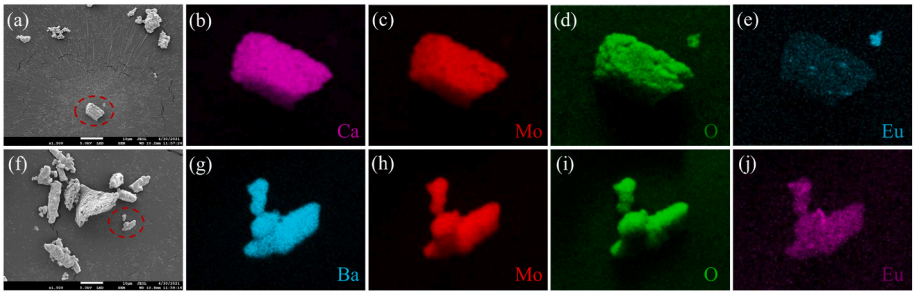

Fig. 2. SEM images and elemental mapping images of representative (a–e) $CaMoO_4$:$0.06Eu^{3+}$ and (f–j) $BaMoO_4$:$0.06Eu^{3+}$ phosphors.

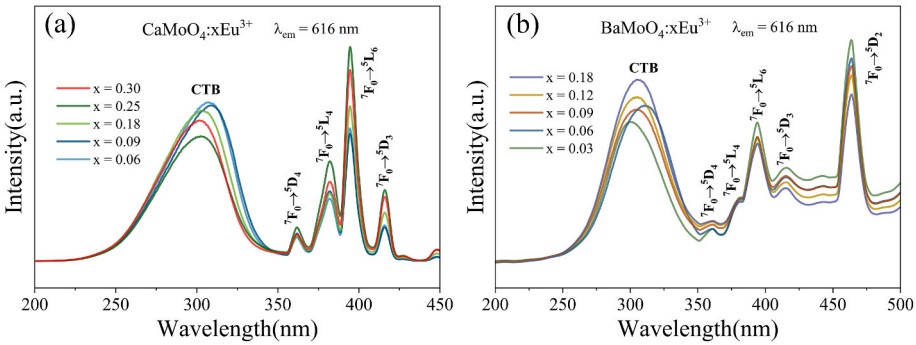

Fig. 3. PLE spectra of (a) $CaMoO_4$:xEu^{3+} and (b) $BaMoO_4$:xEu^{3+} phosphors.

concentration of $CaMoO_4$:Eu^{3+} phosphor is 0.18. In contrast, with the increase in the doping concentration, the Eu^{3+} emission intensity of $BaMoO_4$:Eu^{3+} phosphors increase (Fig. 5(b)), that is, the Eu^{3+} peak doping concentration may be greater than 0.18. In addition, the illustration shows the ET efficiency, which can be calculated as follows [32–34]:

$$\eta_x = 1 - \frac{I_x}{I_{x0}} \quad (1)$$

Here, I_x and I_{x0} represent the emission intensities of the host with and without Eu^{3+} dopant, respectively, and η_x represents the ET efficiency. The highest efficiencies of the two phosphors are 51.89% and 15.29%, respectively.

Generally, electric multipolar interaction and exchange interaction can affect or dominate CQ. To determine the CQ mechanism, the critical distance (R_c) of Eu^{3+} is estimated as follows [30,35–37]:

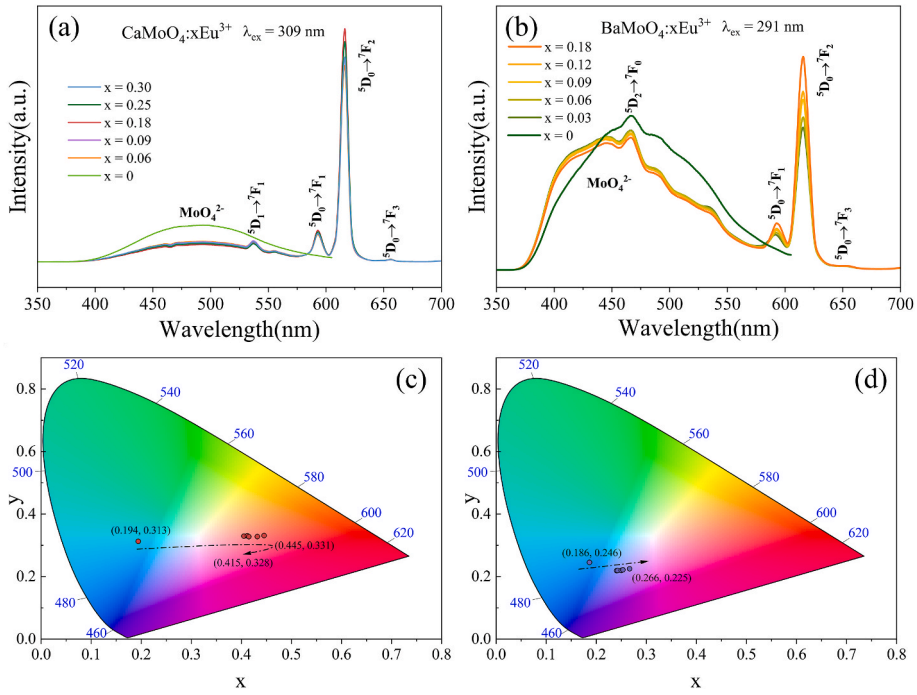

Fig. 4. PL emission spectra of (a) $CaMoO_4:xEu^{3+}$ and (b) $BaMoO_4:xEu^{3+}$ phosphors. CIE chromatic coordinates of (c) $CaMoO_4:xEu^{3+}$ and (d) $BaMoO_4:xEu^{3+}$ phosphors.

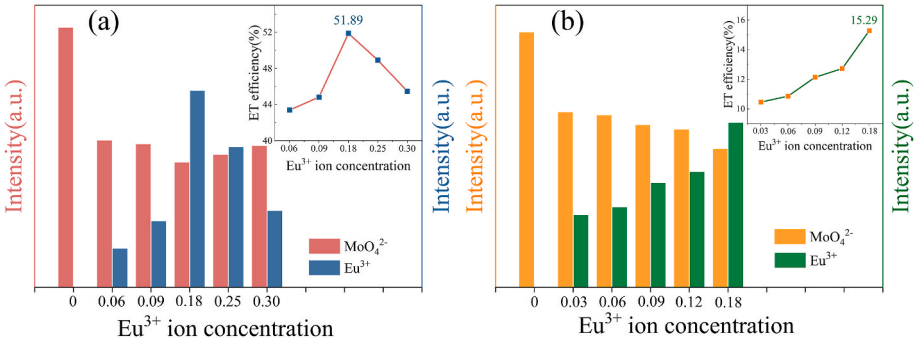

Fig. 5. Comparison of the host and Eu^{3+} emission intensities of (a) $CaMoO_4:xEu^{3+}$ and (b) $BaMoO_4:xEu^{3+}$ phosphors. The corresponding ET efficiency curves are also shown in the inset.

$$R_c \cong 2\left(\frac{3V}{4\pi x_c Z}\right)^{1/3} \quad (2)$$

Here, the cell volume (V), critical concentration (x_c), and cation number (Z) were 312.395 $Å^3$, 0.18, and 4, respectively. Therefore, R_c is estimated to be about 9.39 Å (greater than 5 Å), indicating that the electric multipole interaction plays a dominant role in CQ mechanism. For determining the strength and basic type of multipole interaction, the relationship between the emission intensity and Eu^{3+} doping concentration according to Dexter's theory [38] can be expressed as follows:

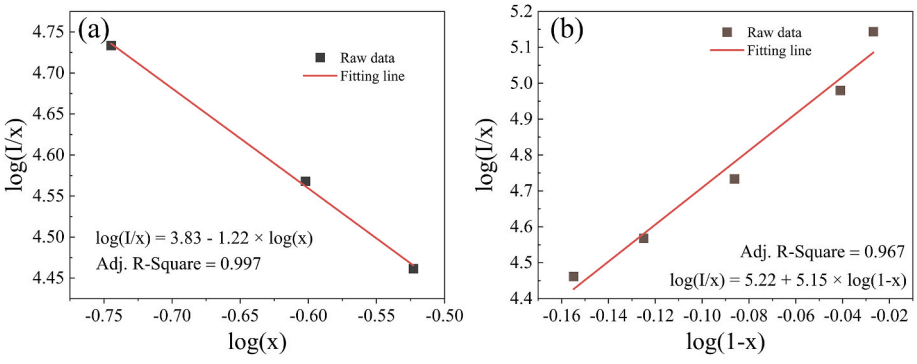

Fig. 6. (a) Plot of log(x) vs log(I/x) and (b) plot of log(I/x) vs log(1-x).

$$\frac{I}{x} = c\left(1 + \beta(x)^{Q/3}\right)^{-1} \quad (3)$$

Here, I, x, and Q represent the PL emission intensity, Eu^{3+} doping concentration, and interaction constant, respectively. c and β are constants. After transformation, the above Eq. (3) can be expressed as follows [36,39]:

$$log(I/x) = C - (Q/3)log(x) \quad (4)$$

Here, C is a constant. Therefore, the curve of log(I/x) vs log(x) after fitting is shown in Fig. 6(a). Its slope is about −1.22, with a Q value of about 3.66. Generally, a Q value of 3 represents exchange interaction, while Q values of 6 represent the dipole–dipole (d–d) interaction. The calculated Q value is about 3, indicating that the CQ of the $CaMoO_4$:Eu^{3+} phosphor results from the combination of d–d interaction and exchange interaction [20,39].

Additionally, the relationship between the activator concentration and emission intensity can be expressed by Eq. (5), which can be rewritten as Eq. (6) [40]:

$$I = Ax(1-x)^Z \quad (5)$$

$$\lg(I/x) = Z\lg(1-x) + C \quad (6)$$

Where, C = lgA is a host-dependent constant and Z is the number of nearest cations around the luminescent center ions. Therefore, Fig. 6(b) shows the dependence of lg (I/x) on lg (1-x). The calculated Z value is 5.15 and the critical quenching concentration 1/(1 + Z) is 0.163, which is close to the experimental critical quenching concentration 0.18. It proves the reliability of the above analysis of quenching concentration mechanism.

The luminescent behavior of Eu^{3+} is extremely sensitive to the central asymmetry of its sites in the host lattice. Therefore, the central asymmetry of Eu^{3+} is calculated using the following Eq. (7):

$$R = I\left({}^5D_0 \rightarrow {}^7F_2\right) / I\left({}^5D_0 \rightarrow {}^7F_1\right) \quad (7)$$

Fig. 7 shows the relationship between R and Eu^{3+} concentration of phosphors. On the one hand, the R value for the $CaMoO_4$:Eu^{3+} phosphor increases first and then decreases with the increase in the Eu^{3+} content, and the turning point is at x = 0.18, which is the CQ point. In addition, the variation of Eu^{3+} emission intensity, ET efficiency, and R-value with Eu^{3+} content are nearly consistent, attributed to the fact that the ${}^5D_0 \rightarrow {}^7F_2$ transition of Eu^{3+} almost dominates its emission. With the increase in the Eu^{3+} content, the R value of $BaMoO_4$:Eu^{3+} increases, indicating that the central asymmetry of Eu^{3+} is stronger at a high doping concentration.

In addition, the decay curves of all phosphors were further recorded to examine the luminescence kinetics under an excitation wavelength of 309 nm or 291 nm (Fig. 8). The lifetime of phosphors can be estimated as follows:

$$I(t) = Aexp\left(-\frac{t}{\tau}\right) + B \quad (8)$$

The lifetimes of $CaMoO_4$:Eu^{3+} phosphors were estimated to be about 0.428, 0.420, 0.431, 0.425, and 0.432 ms (x = 0.06, 0.09, 0.18, 0.25, and 0.3, respectively) by single-exponential function fitting, and the lifetimes of $BaMoO_4$:Eu^{3+} phosphors were about 0.533, 0.524, 0.522, 0.534, and 0.505 ms (x = 0.03, 0.06, 0.09, 0.12, ad 0.18, respectively).

3.3. Temperature measurement sensitivity analysis

Thermal stability of phosphors is a key parameter for their practical applications. Therefore, the temperature-dependent PL emission spectra of the representative $CaMoO_4$:$0.09Eu^{3+}$ and $BaMoO_4$:$0.03Eu^{3+}$ phosphors are recorded (Fig. 9(a) and (b)). Clearly, the position and shape of the emission spectra do not change with the increase in the temperature. For $CaMoO_4$:$0.09Eu^{3+}$ phosphor, the inset revealed that the emission intensity of MoO_4^{2-} group first decreases and then increases, corresponding to 46.98% (423 K) and 101.31% (573 K) of that at room temperature, respectively, while the emission intensity of Eu^{3+} exhibits an opposite trend, corresponding to 154.52% (423 K) and 98.77% (573 K) of that at room temperature, respectively. The abnormal enhancement of Eu^{3+} emission intensity is attributed to the lattice defects caused by the heterovalent substitution ($3Ca^{2+} \rightarrow 2Eu^{3+} + 1V_{Ca}$, V_{Ca} represents Ca^{2+} vacancy) of ions and the high-concentration defects caused by heating [41–43]. For the phosphor prepared by solid-state method, it contains a higher concentration of defects [14,43–45]. The concentration of defects is further increased due to heterovalent substitution and heating, and these defects can serve as electron capture centers. Hence, the residual energy of the excited electrons is transferred and stored in Eu^{3+}, and the emission increase caused by defects is greater than the emission loss caused by non-radiative transitions at high temperatures, resulting in the enhancement of red luminescence [26,42,43]. At temperatures of greater than 423 K, the emission increase caused by defects started to be less than the emission loss caused by non-radiative transitions in quantity, and thermal quenching becomes normal. In addition, owing to the abnormal luminescent enhancement, $CaMoO_4$:$0.09Eu^{3+}$ may be considered for potential applications at high temperatures.

For $BaMoO_4$:$0.03Eu^{3+}$ phosphor, the Eu^{3+} emission intensity decreases with the increase in temperature, while the MoO_4^{2-} group exhibits an opposite trend, corresponding to 40.23% and 112.46% at 573 K, respectively. According to the Struck–Fonger model and Wang's study [26], the electrons are excited to the highest excited state ${}^5L_6$, and the excited electrons are then transferred along the CTS to the lower energy level ${}^5D_J$ (J = 1, 2, 3) and subsequently transferred to ${}^5D_0$ via cross-relaxation. With the increase in the temperature, the excited electrons overcome the energy barrier ΔE_0 via feat of phonons, and some electrons reach ${}^5D_J$, and some electrons relax to ${}^7F_J$. The theory explains the thermal quenching mechanism well and the increase in the ${}^5D_J$ emission intensity. Since the emission intensity of MoO_4^{2-} group is

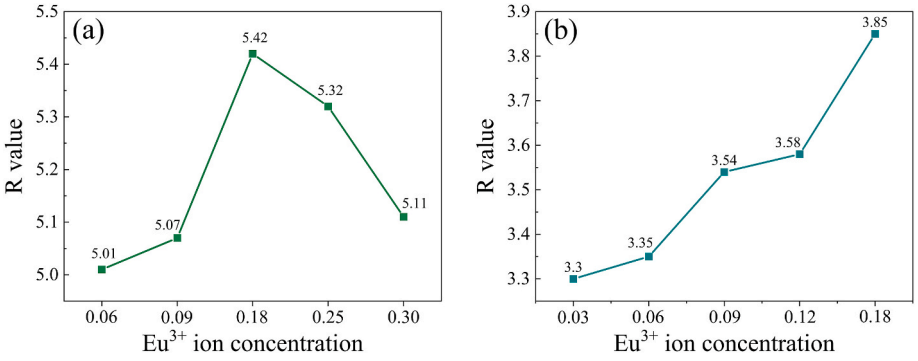

Fig. 7. Plot between R value and Eu^{3+} concentration of (a) $CaMoO_4$:xEu^{3+} and (b) $BaMoO_4$:xEu^{3+} phosphors.

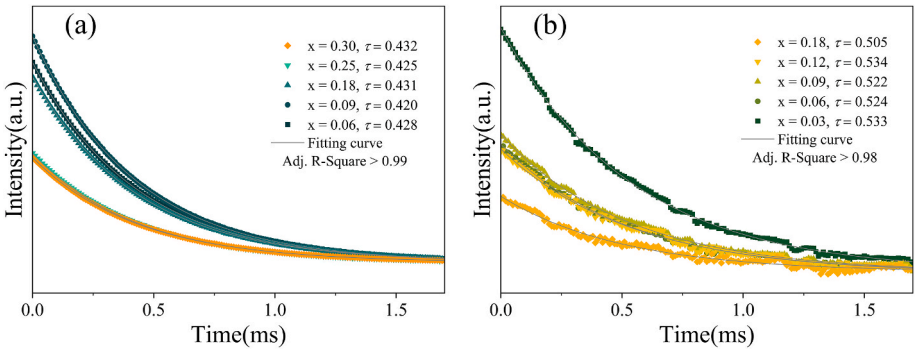

Fig. 8. Luminescent decay curves of (a) $CaMoO_4$:xEu^{3+} and (b) $BaMoO_4$:xEu^{3+} phosphors.

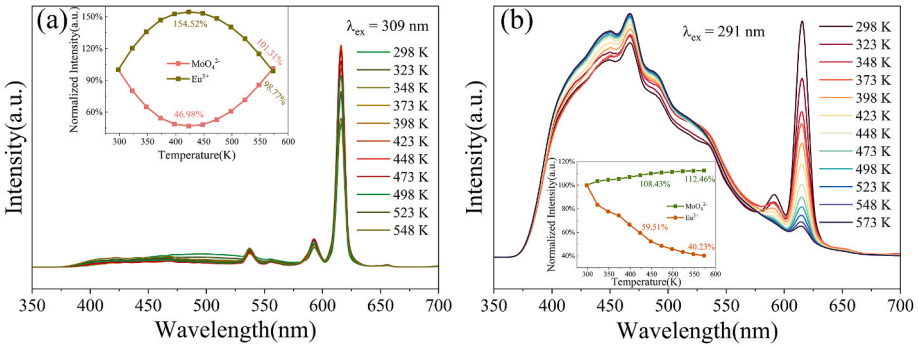

Fig. 9. Temperature-dependent PL emission spectra of (a) $CaMoO_4$:0.09Eu^{3+} and (b) $BaMoO_4$:0.03Eu^{3+} phosphors.

clearly greater than that of Eu^{3+} ^5D_J, and the latter is overlaid by the former on the diagram, as a result, the emission intensity of MoO_4^{2-} group increases with the increase in temperature. The increase in the emission intensity of MoO_4^{2-} group is actually the increase in Eu^{3+} ^5D_J emission intensity.

In addition, $AMoO_4$:Eu^{3+} phosphors can be used to design non-contact temperature sensors based on NTCL ($^3T_{1,\,2}$ of the host and $^5D_0$ of Eu^{3+}) and ET effects [20,28]. Fig. 10(a) and (b) shows the plot and fitting of the relationship between FIR and the temperature. The fitting relationship of FIR is expressed as follows [46–49]:

$$FIR_{Ca} = A_1 + B_1T + C_1T^2 = 9.295 - 0.042T + 4.847 \times 10^{-5}T^2 \quad (9)$$

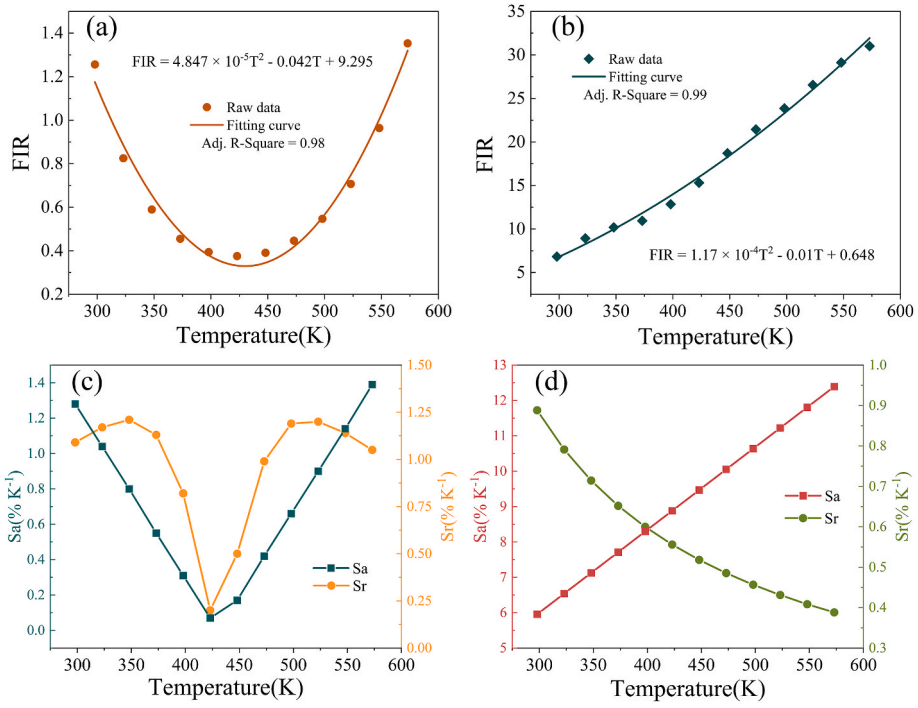

Fig. 10. FIR as well as Sa and Sr values of (a, c) $CaMoO_4$:0.09Eu^{3+} and (b, d) $BaMoO_4$:0.03Eu^{3+} phosphors.

$$FIR_{Ba} = A_2 + B_2T + C_2T^2 = 0.648 - 0.01T + 1.17 \times 10^{-4}T^2 \quad (10)$$

Typically, the Sa and Sr values of the phosphors are derived and calculated from the following expressions [10,49,50]:

$$Sa = \left|\frac{d(FIR)}{dT}\right| = B + 2CT \quad (11)$$

$$Sr = \left|\frac{1}{FIR} \times \frac{d(FIR)}{dT}\right| \times 100\% \quad (12)$$

Fig. 10(c) and (d) shows the calculation results of Sa and Sr values of representative phosphors. Clearly, with the increase in the temperature, the variation trend in Sa value is the same as that of the corresponding FIR value. The large difference in Sa values between the two phosphors is attributed to the large difference in FIR. Notably, $CaMoO_4$:0.09Eu^{3+} phosphor exhibits two peak Sa values of 1.28 %K^{-1} (273 K) and 1.39 %K^{-1} (573 K), respectively. As the FIR value is fitted using a quadratic function, the Sa value at each temperature is well known to be the absolute value of the slope of the tangent at that point (Eq. (11)). However, its Sr value changes anomalously with temperature, and there are two optimum Sr values in the temperature range of 1.21 %K^{-1} (348 K) and 1.20 %K^{-1} (523 K), respectively. The strange Sa and Sr curves of $CaMoO_4$:0.09Eu^{3+} phosphor are related to its abnormal thermal quenching. The optimum Sa and Sr values of the $BaMoO_4$:0.03Eu^{3+} phosphor are 12.39 %K^{-1} (573 K) and 0.89 %K^{-1} (273 K), respectively. Additionally, the two phosphors exhibit good temperature sensitivity compared to other people 's work [11,49,51,52].

Previously, our group has hypothesized that the Sa of phosphors is negatively related to the central asymmetry of Eu^{3+} and that the peak Sr value is more inclined to a suitable ionic center asymmetry. Therefore, the relationship between R value and temperature of $CaMoO_4$:0.09Eu^{3+} and $BaMoO_4$:0.03Eu^{3+} phosphors is plotted (Fig. 11). Clearly, in this study, the Sa of the two phosphors is negatively related to Eu^{3+} central asymmetry. The R values corresponding to the peak Sr value of $CaMoO_4$:0.09Eu^{3+} phosphor are 6.02 and 5.37, respectively. In other words, the peak Sr value is more inclined to a suitable ionic center asymmetry, and the R value corresponding to the peak Sr value of $BaMoO_4$:0.03Eu^{3+} phosphor is 3.12 (within the monitoring temperature range). The above conclusions are consistent with those reported in our previous study [19]. In addition, with the increase in temperature, the R value of $CaMoO_4$:0.09Eu^{3+} phosphor increases first and then decreases, possibly related to the abnormal thermal quenching, because the variation tendency of R value of Eu^{3+} with temperature is basically consistent with its emission intensity, and the $^5D_0 \rightarrow {}^7F_2$ transition dominates the Eu^{3+} emission. The increase in the Eu^{3+} central asymmetry may be attributed to the increase in the defect concentration caused by heating, as this will lead to more significant lattice distortion [42].

4. Conclusion

In this study, a range of $AMoO_4$:Eu^{3+} (A = Ca and Ba) optical thermometers based on FIR with a pair of NTCL as well as ET effect were designed and synthesized. Their crystal structures, luminescent behaviors, temperature measurement sensitivities, and influencing factors were examined in detail. These phosphors exhibited excitation at wavelengths of 309 and 291 nm, respectively, with clearly observed host emissions and characteristic emissions of Eu^{3+}. The CQ of $CaMoO_4$:xEu^{3+} phosphor at x = 0.18 is attributed to the d–d interaction and exchange interaction, while CQ does not occur in $BaMoO_4$:Eu^{3+} phosphor. In addition, since the $^5D_0 \rightarrow {}^7F_2$ transition almost dominates Eu^{3+} emission, the variation of Eu^{3+} emission intensity, ET efficiency, and the R value with Eu^{3+} content are nearly consistent. Then, temperature-dependent PL emission spectra of representative $CaMoO_4$:0.09Eu^{3+} and $BaMoO_4$:0.03Eu^{3+} phosphor were recorded. The former exhibited abnormal thermal quenching, and the emission intensities of Eu^{3+} were 154.52% (423 K) and 98.77% (573 K) of the emission intensity at room temperature, indicative of good thermal stability. In addition, the possibility of using these two phosphors as luminescent thermometers was investigated: these phosphors exhibited good temperature sensing performance. The former exhibits two peak Sa (1.28 %K^{-1}, 1.39 %K^{-1}) and Sr (1.21 %K^{-1}, 1.20 %K^{-1}) values, respectively, while the latter exhibits peak Sa and Sr values of 12.39 %K^{-1} and 0.89 %K^{-1}, respectively. Finally, the effect of the Eu^{3+} central asymmetry on temperature measurement sensitivity of optical thermometers was investigated. The Sa value was negatively related to the Eu^{3+} central asymmetry, while the Sr value was more inclined to the appropriate ionic center asymmetry. Based on the above results, the $AMoO_4$:Eu^{3+} (A = Ca and Ba) phosphors were confirmed to be used as optical thermometers.

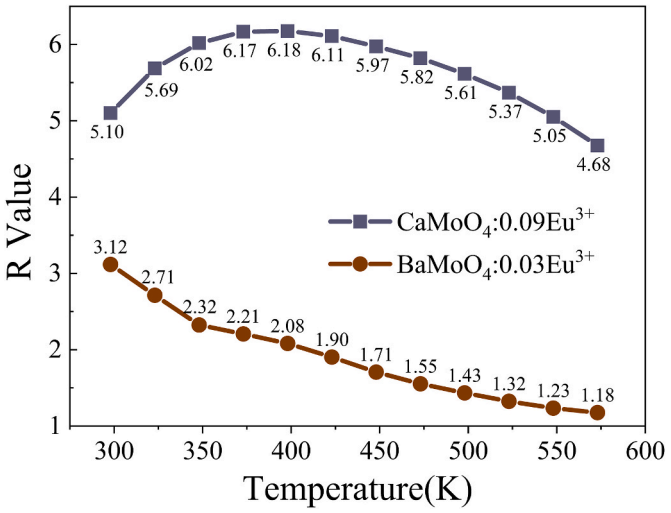

Fig. 11. Temperature dependence of R of $CaMoO_4$:0.09Eu^{3+} and $BaMoO_4$:0.03Eu^{3+} phosphors.

Declaration of competing interest

The authors declare that they have no known competing financial interests or personal relationships that could have appeared to influence the work reported in this paper.

Acknowledgments

The work was supported by the program of Science and Technology International Cooperation Project of Qinghai province (No. 2022-HZ-807) and the National Natural Science Foundation of China (Grant No. 51802172), and was carried out within the framework of the Strategic Academic Leadership Program "Priority-2030" for the Siberian Federal University.

References

[1] H. Suo, C. Guo, T. Li, Broad-Scope thermometry based on dual-color modulation up-conversion phosphor $Ba_5Gd_8Zn_4O_{21}$:Er^{3+}/Yb^{3+}, J. Phys. Chem. C 120 (2016) 2914–2924.
[2] B.P. Kore, A. Kumar, L. Erasmus, R.E. Kroon, J.J. Terblans, S.J. Dhoble, H.C. Swart, Energy transfer mechanisms and optical thermometry of $BaMgF_4$:Yb^{3+},Er^{3+} phosphor, Inorg. Chem. 57 (2018) 288–299.
[3] Y. Hua, J.S. Yu, Synthesis and luminescent properties of near-UV excited NaLa$(MoO_4)_2$:Er^{3+} phosphors for multifunctional applications, J. Alloys Compd. 811 (2019), 152050.
[4] A.A. Ansari, A.K. Parchur, M.K. Nazeeruddin, M.M. Tavakoli, Luminescent lanthanide nanocomposites in thermometry: chemistry of dopant ions and host matrices, Coord. Chem. Rev. 444 (2021), 214040.
[5] C. Wang, Y. Jin, R. Zhang, Q. Yao, Y. Hu, A review and outlook of ratiometric optical thermometer based on thermally coupled levels and non-thermally coupled levels, J. Alloys Compd. 894 (2022), 162494.
[6] H. Liu, L. Mei, L. Liao, Y. Zhang, Q. Guo, T. Zhou, Y. Wang, L. Li, Strategy for realizing ratiometric optical thermometry via efficient Tb^{3+}-Mn^{2+} energy transfer

in novel apatite-type phosphor $Ca_9Tb(PO_4)_5(SiO_4)F_2$, J. Alloys Compd. 770 (2019) 1237–1243.
[7] J. Xue, H.M. Noh, B.C. Choi, S.H. Park, J.H. Kim, J.H. Jeong, P. Du, Dual-functional of non-contact thermometry and field emission displays via efficient $Bi^{3+} \rightarrow Eu^{3+}$ energy transfer in emitting-color tunable $GdNbO_4$ phosphors, Chem. Eng. J. 382 (2020), 122861.
[8] X. Zhang, Z. Zhu, Z. Guo, Z. Sun, Y. Chen, A ratiometric optical thermometer with high sensitivity and superior signal discriminability based on $Na_3Sc_2P_3O_{12}$: Eu^{2+}, Mn^{2+} thermochromic phosphor, Chem. Eng. J. 356 (2019) 413–422.
[9] P. Du, Y. Hua, J.S. Yu, Energy transfer from VO_4^{3-} group to Sm^{3+} ions in $Ba_3(VO_4)_2$: 3xSm^{3+} microparticles: a bifunctional platform for simultaneous optical thermometer and safety sign, Chem. Eng. J. 352 (2018) 352–359.
[10] X. Yang, X. Li, Y. Li, J. Shang, B. Ma, Effect of energy transfer and local crystal field perturbation on the thermometric sensitivity of Ga-Tb-Eu ternary emission system, Ceram. Int. 48 (2022) 684–693.
[11] P. Khajuria, A.K. Bedyal, M. Manhas, H.C. Swart, F. Durani, V. Kumar, Spectral, surface and thermometric investigations of upconverting Er^{3+}/Yb^{3+} co-doped $Na_3Y(PO_4)_2$ phosphor, J. Alloys Compd. 877 (2021), 160327.
[12] H. Suo, X. Zhao, Z. Zhang, T. Li, E.M. Goldys, C. Guo, Constructing multiform morphologies of YF: Er^{3+}/Yb^{3+} up-conversion nano/micro-crystals towards sub-tissue thermometry, Chem. Eng. J. 313 (2017) 65–73.
[13] X. Wang, Y. Wang, Y. Bu, X. Yan, J. Wang, P. Cai, T. Vu, H.J. Seo, Influence of doping and excitation powers on optical thermometry in Yb^{3+}-Er^{3+} doped $CaWO_4$, Sci. Rep. 7 (2017), 43383.
[14] I. Gupta, S. Singh, S. Bhagwan, D. Singh, Rare earth (RE) doped phosphors and their emerging applications: a review, Ceram. Int. 47 (2021) 19282–19303.
[15] A.A. Ansari, M.R. Muthumareeswaran, R. Lv, Coordination chemistry of the host matrices with dopant luminescent Ln^{3+} ion and their impact on luminescent properties, Coord. Chem. Rev. 466 (2022), 214584.
[16] Y. Zhang, L. Mei, S.M. Aksenov, D. Deyneko, H. Liu, D. Zhang, Z. Huang, New apatite-type phosphor $Ca_9La(PO_4)_5(SiO_4)F_2$:Tb^{3+},Dy^{3+} with improved color rendering index, J. Am. Ceram. Soc. 103 (2019) 2602–2609.
[17] H. Liu, L. Liao, Y. Zhang, S. Aksenov, N. Liu, Q. Guo, D. Deyneko, T. Wang, L. Mei, C. Sun, Computational analysis of apatite-type compounds for band gap engineering: DFT calculations and structure prediction using tetrahedral substitution, Rare Met. 40 (2021) 3694–3700.
[18] Q. Liu, M. Zhang, Z. Ye, X. Wang, Q. Zhang, B. Wei, Structure variation and luminescence enhancement of BaLaMg(Sb, Nb)O_6:Eu^{3+} double perovskite red phosphors based on composition modulation, Ceram. Int. 45 (2019) 7661–7666.
[19] H. Gao, M.S. Molokeev, Q. Chen, X. Yang, X. Wang, B. Ma, Effect of ligand environment of rare-earth ions on temperature measurement performance of $SrAO_4$:xEu^{3+} (A = Mo and W) phosphors, Ceram. Int. 48 (2022) 36835–36844.
[20] F.M. Emen, V.E. Kafadar, N. Korozlu, R.E. Demirdogen, The photoluminescence and thermoluminescence characteristics of the Eu^{3+} doped $CaMoO_4$: detailed kinetic analysis of TL glow curves, J. Lumin. 222 (2020), 117130.
[21] L. He, X. Zou, T. Wang, Q. Zheng, J. Liao, C. Xu, Y. Liu, D. Lin, Cation-induced variation of micromorphology and luminescence properties of tungstate phosphors by a hydrothermal method, Inorg. Chem. 55 (2016) 12944–12952.
[22] X. Huang, C. He, X. Zhu, C. Yang, Y. Liu, M. Wu, X. Min, R. Mi, Z. Huang, Synthesis and characterization of Eu^{3+}-doped $RbCaLa(VO_4)_2$ phosphors and influence of temperature on fluorescence properties, Ceram. Int. 47 (2021) 32130–32137.
[23] D. Liu, Y. Liu, Y. Zhu, S. Ye, B. Shaojie, Enhancement of luminescence properties of Zn(W–Mo)O_4:Eu^{3+} red phosphors by co-doped charge compensators A^+(Li^+, Na^+, K^+), Ceram. Int. 47 (2021) 28021–28031.
[24] T. Dai, G. Ju, Y. Lv, Y. Jin, H. Wu, Y. Hu, Luminescence properties of novel dual-emission (UV/red) long afterglow phosphor $LiYGeO_4$: Eu^{3+}, J. Lumin. 237 (2021), 118193.
[25] X. Guo, S. Song, X. Jiang, J. Cui, Y. Li, W. Lv, H. Liu, Y. Han, L. Wang, Functional applications and luminescence properties of emission tunable phosphors $CaMoO_4$@SiO_2:Ln^{3+} (Ln=Eu, Tb, Dy), J. Alloys Compd. 857 (2021), 157515.
[26] S. Wang, Y. Xu, T. Chen, W. Jiang, J. Liu, X. Zhang, W. Jiang, L. Wang, A novel red phosphor $Ba_2La_4Y_4(SiO_4)_6O_2$:Eu^{3+} with high quantum yield and thermal stability for warm white LEDs, J. Alloys Compd. 789 (2019) 381–391.
[27] A.R. Sharits, J.F. Khoury, P.M. Woodward, Evaluating $NaREMgWO_6$ (RE = La, Gd, Y) doubly ordered double perovskites as Eu^{3+} phosphor hosts, Inorg. Chem. 55 (2016) 12383–12390.
[28] S. Li, L. Yu, J. Sun, X. Man, Synthesis and photoluminescent characteristics of Eu^{3+}-doped $MMoO_4$ (M=Sr, Ba) nanophosphors by a hydrothermal method, J. Rare Earths 35 (2017) 347–3355.
[29] Y. Wang, J. Ding, Z. Zhao, Y. Wang, A cerium doped scandate broad orange-red emission phosphor and its energy transfer-dependent concentration and thermal quenching character, Inorg. Chem. 57 (2018) 14542–14553.
[30] Y. Hua, W. Ran, J.S. Yu, Excellent photoluminescence and cathodoluminescence properties in Eu^{3+}-activated Sr_2LaNbO_6 materials for multifunctional applications, Chem. Eng. J. 406 (2021), 127154.
[31] F. Zhao, H. Cai, Z. Song, Q. Liu, Structural confinement for Cr^{3+} activators toward efficient near-infrared phosphors with suppressed concentration quenching, Chem. Mater. 33 (2021) 3621–3630.
[32] S.A. Khan, N.Z. Khan, M. Sohail, J. Ahmed, N. Alhokbany, S.M. Alshehri, X. Xu, J. Zhu, S. Agathopoulos, Modern aspects of strategies for developing single-phase broadly tunable white light-emitting phosphors, J. Mater. Chem. C 9 (2021) 13041–13071.
[33] C.H. Huang, T.W. Kuo, T.M. Chen, Novel red-emitting phosphor $Ca_9Y(PO_4)_7$:Ce^{3+}, Mn^{2+} with energy transfer for fluorescent lamp application, ACS Appl. Mater. Interfaces 2 (2010) 1395–1399.
[34] B. Zheng, X. Zhang, D. Zhang, F. Wang, Z. Zheng, X. Yang, Q. Yang, Y. Song, B. Zou, H. Zou, Ultra-wideband phosphor $Mg_2Gd_8(SiO_4)_6O_2$:Ce^{3+},Mn^{2+}: energy transfer and pressure-driven color tuning for potential applications in LEDs and pressure sensors, Chem. Eng. J. 427 (2022), 131897.
[35] Y. Alajlani, N. Can, Novel Dy and Sm activated $BaSi_2O_5$ phosphors: insights into the structure, intrinsic and extrinsic luminescence, and influence of doping concentration, J. Lumin. 230 (2021), 117718.
[36] Y. Hua, J.S. Yu, Strong green emission of erbium(III)-activated La_2MgTiO_6 phosphors for solid-state lighting and optical temperature sensors, ACS Sustainable Chem. Eng. 9 (2021) 5105–5115.
[37] X. Wu, L. Du, Q. Ren, O. Hai, Study on the color tunability and energy transfer mechanism in Tm^{3+}/Dy^{3+} co-doped $LiLaSiO_4$ phosphors, Ceram. Int. 47 (2021) 28384–28399.
[38] D.L. Dexter, J.H. Schulman, Theory of concentration quenching in inorganic phosphors, J. Chem. Phys. 22 (1954) 1063–1070.
[39] X. Zhang, J. Zhang, Z. Dong, J. Shi, M. Gong, Concentration quenching of Eu^{2+} in a thermal-stable yellow phosphor Ca_2BO_3Cl:Eu^{2+} for LED application, J. Lumin. 132 (2012) 914–918.
[40] L. Li, W. Chang, W. Chen, Z. Feng, C. Zhao, P. Jiang, Y. Wang, X. Zhou, A. Suchocki, Double perovskite $LiLaMgWO_6$:Eu^{3+} novel red-emitting phosphors for solid sate lighting: synthesis, structure and photoluminescent properties, Ceram. Int. 43 (2017) 2720–2729.
[41] Z. Zhou, H. Zhu, X. Huang, Y. She, Y. Zhong, J. Wang, M. Liu, W. Li, M. Xia, Anti-thermal-quenching, color-tunable and ultra-narrow-band cyan green-emitting phosphor for w-LEDs with enhanced color rendering, Chem. Eng. J. 433 (2022), 134079.
[42] Y.H. Kim, P. Arunkumar, B.Y. Kim, S. Unithrattil, E. Kim, S.H. Moon, J.Y. Hyun, K. H. Kim, D. Lee, J.S. Lee, W.B. Im, A zero-thermal-quenching phosphor, Nat. Mater. 16 (2017) 543–550.
[43] X. Qin, X. Liu, W. Huang, M. Bettinelli, X. Liu, Lanthanide-activated phosphors based on 4f-5d optical transitions: theoretical and experimental aspects, Chem. Rev. 117 (2017) 4488–4527.
[44] S.K. Gupta, R.M. Kadam, P.K. Pujari, Lanthanide spectroscopy in probing structure-property correlation in multi-site photoluminescent phosphors, Coord. Chem. Rev. 420 (2020), 213405.
[45] Z. Zhou, Y. Li, M. Peng, Near-infrared persistent phosphors: synthesis, design, and applications, Chem. Eng. J. 399 (2020), 125688.
[46] Z. Zheng, J. Zhang, X. Liu, R. Wei, F. Hu, H. Guo, Luminescence and self-referenced optical temperature sensing performance in $Ca_2YZr_2Al_3O_{12}$:Bi^{3+},Eu^{3+} phosphors, Ceram. Int. 46 (2020) 6154–6159.
[47] H. Lu, H. Hao, G. Shi, Y. Gao, R. Wang, Y. Song, Y. Wang, X. Zhang, Optical temperature sensing in β-$NaLuF_4$:Yb^{3+}/Er^{3+}/Tm^{3+} based on thermal, quasi-thermal and non-thermal coupling levels, RSC Adv. 6 (2016) 55307–55311.
[48] D. Chen, Z. Wan, S. Liu, Highly sensitive dual-Phase nanoglass-ceramics self-calibrated optical thermometer, Anal. Chem. 88 (2016) 4099–4106.
[49] L. Li, X. Tang, Z. Wu, Y. Zheng, S. Jiang, X. Tang, G. Xiang, X. Zhou, Simultaneously tuning emission color and realizing optical thermometry via efficient $Tb^{3+} \rightarrow Eu^{3+}$ energy transfer in whitlockite-type phosphate multifunctional phosphors, J. Alloys Compd. 780 (2019) 266–275.
[50] Z. Wang, H. Jiao, Z. Fu, Investigating the luminescence behaviors and temperature sensing properties of Rare-Earth-doped $Ba_2In_2O_5$ phosphors, Inorg. Chem. 57 (2018) 8841–8849.
[51] Z. Zhang, J. Yan, Q. Zhang, G. Tian, W. Jiang, J. Huo, H. Ni, L. Li, J. Li, Enlarging sensitivity of fluorescence intensity ratio-type thermometers by the interruption of the energy transfer from a sensitizer to an activator, Inorg. Chem. 61 (2022) 16484–16492.
[52] Y. Jiang, Y. Tong, S. Chen, W. Zhang, F. Hu, R. Wei, H. Guo, A three-mode self-referenced optical thermometry based on up-conversion luminescence of Ca_2MgWO_6:Er^{3+},Yb^{3+} phosphors, Chem. Eng. J. 413 (2021), 127470.